Simultaneous label-free two-photon fluorescence and second-harmonic generation microscopy for visualization of mouse pulmonary alveoli

Yanyan Deng[a], Yifan Qin*[b], Zhibin Zhang[b], Zeming Zhang[b], Yuanqin Xia*[a,b]
[a]Center for Advanced Laser Technology, Hebei University of Technology, 5340 Xiping Street, Tianjin, China 300401; [b]National Key Laboratory of Science and Technology on Tunable Laser, Harbin Institute of Technology, 2 Yikuang Street, Harbin, China 150080

ABSTRACT

We demonstrate a label-free imaging system capable of generating two-photon fluorescence (TPF) and second-harmonic generation (SHG) signals simultaneously, using a wavelength-tunable mode-locked Ti:Sapphire laser. TPF and SHG images are acquired at two wavelength ranges. One is between 415 nm and 455 nm, and the other is between 495 nm and 635 nm. The capability of the imaging system is demonstrated by performing simultaneous TPF and SHG imaging of freshly excised mouse lung lobes. At 870 nm excitation, the microenvironment of pulmonary alveoli is revealed by TPF from elastin fibers and SHG from collagen fibers. Macrophages residing inside apparent alveolar lumens are also identified by autofluorescence.

Keywords: two-photon fluorescence, second-harmonic generation, label-free microscopy, nonlinear microscopy, mouse tissues

1. INTRODUCTION

Nonlinear optical microscopy has been proved to be a well-established technique based on nonlinear interactions between light and matter[1,2]. In a nonlinear optical process, the emission intensity has a quadratic or high-order dependence on the excitation intensity, which ensures that the signal collected out of the focal volume reaches its minimum. Thus, the nonlinear optical microscopy has submicron three-dimensional spatial resolution with higher signal-to-noise ratio and less out-of-focus photobleaching, compared with confocal microscopy[3–7]. In addition, using near infrared (NIR) excitation wavelengths also increases penetration depth into scattering specimens, which is significant for biological imaging[8,9]. Several nonlinear processes have been applied for biological microscopy, including two-photon fluorescence (TPF)[10–13], three-photon fluorescence (ThPF)[14,15], second-harmonic generation (SHG)[16,17], third-harmonic generation (THG)[18], coherent anti-Stokes Raman scattering (CARS)[19,20], and stimulated Raman scattering (SRS)[21].

TPF microscopy is the most preferred nonlinear microscopy for biological imaging since 1990[10], thanks to its simpler setup compared with CARS and SRS microscopy, and its superior ability to image a wider range of specimens compared to other multiphoton microscopy techniques, i.e., ThPF, SHG, and THG. Some intrinsic fluorescent biomolecules in biological tissues can be applied for imaging without the need of exogenous biomarkers, which ensures that TPF microscopy is a label-free technique. These biomolecules called endogenous fluorophores exist in both intracellular scale and extracellular matrix of biological tissues[2]. The most widely used intracellular fluorophores are metabolic coenzymes, which include reduced nicotinamide adenine dinucleotide (NADH) and flavin adenine dinucleotide (FAD). NADH and FAD are the main electron donor and acceptor of the electron transport chain in cells, respectively. Visualization of cells has been achieved by TPF imaging of NADH and FAD[8], such as neurons, macrophages, and muscle cells. Investigations of physiological processes have also been demonstrated by using autofluorescence derived from NADH and FAD[22], such as cell differentiation and cancer development. Concerning the extracellular matrix, visualization of autofluorescent proteins, such as elastin, collagen, and keratin, has been achieved by using TPF microscopy to diagnose diseases[23], such as asthma and pulmonary fibrosis.

*qinyifanhit@gmail.com, qinyifan@hit.edu.cn; phone +(86)151-1466-3136; www.researchgate.net/profile/Yifan_Qin
*xiayq@hebut.edu.cn; phone (+86)132-0763-4170

Advanced Optical Imaging Technologies III, edited by Xiao-Cong Yuan, P. Scott Carney, Kebin Shi, Proceedings of SPIE Vol. 11549, 1154916 · © 2020 SPIE
CCC code: 0277-786X/20/$21 · doi: 10.1117/12.2573614

Although TPF is the most widely used nonlinear process for biological microscopy, the first nonlinear label-free microscope is based on SHG[9]. Photons are scattered by molecules in the process of SHG, rather than absorbed in the process of TPF. SHG emitters are required to be spatially organized in non-centrosymmetric structures to avoid cancellation. In biological materials (e.g., collagen and myosin) with such structures, signal of SHG could be very intense. In practice, the structures of collagen containing tissues, such as skin, tendon, and lung, have been revealed by SHG microscopy[16]. Meanwhile, pathological processes of liver fibrosis and hypertrophic scar development have been investigated by SHG imaging of collagen[17]. SHG from collagen is applied more frequently for microscopy than TPF, as it's easier to generate SHG from collagen in most biological tissues with NIR excitation.

Both the research works on TPF and SHG microscopy have practical significances. However, we should also notice that only one kind of information, i.e., physiological or structural information from biological samples, can be collected by these two modalities. A combination of these two modalities will surely obtain more informative and comprehensive images. Recently, we demonstrated high-speed TPF microscopy systems based on two-dimensional laser scanning[24,25]. In this paper, we demonstrate a label-free imaging system capable of generating TPF and SHG signals simultaneously, using a wavelength-tunable mode-locked Ti:Sapphire laser as the excitation source. The imaging system has the advantages of combining two nonlinear imaging modalities to obtain more biological information from unstained samples, and eliminating possible artifacts from sample motion or laser power fluctuation. We demonstrate the capability of the system by performing simultaneous label-free TPF and SHG imaging of freshly excised mouse lung lobes at 870 nm excitation. Signals are collected by detection channels at two wavelength ranges. One is between 415 nm and 455 nm, and the other is between 495 nm and 635 nm. TPF and SHG images of mouse pulmonary alveoli are pseudo-colored, superimposed, and used to investigate the morphologies of these tissues.

2. EXPERIMENTAL SETUP

The experimental setup is shown in Figure 1. A mode-locked Ti:Sapphire laser (Tsunami, Spectra-Physics) is used as the excitation source for simultaneous TPF and SHG microscopy. It generates pulses with 80 MHz repetition rate and 100 fs duration, and its center wavelength is tunable between 700 nm and 1000 nm. A Fabry isolator is applied to minimize back-reflection. The power and the polarization of the laser source can be tuned by rotating the half-wave plates (WPH05M-850, Thorlabs) placed before (HWP1) and after (HWP2) the Fabry isolator, respectively.

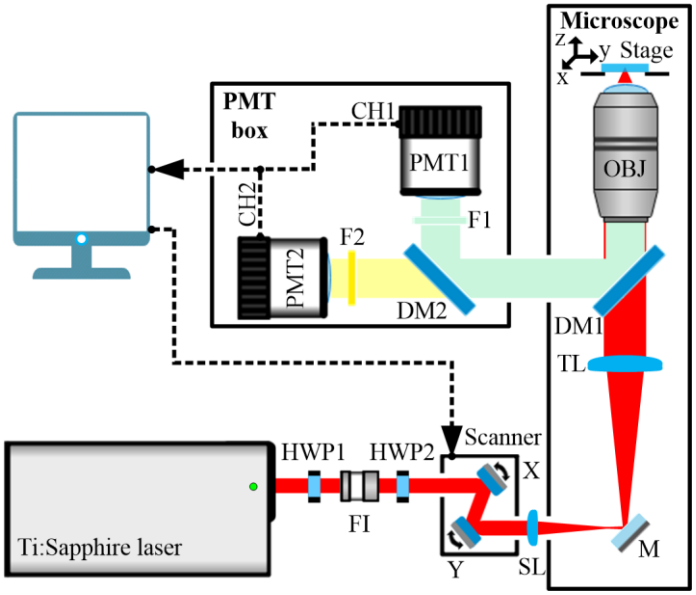

Figure 1. Experimental setup of a simultaneous label-free TPF and SHG imaging system. The excitation beam is shown in red, and generated signals at different wavelengths are shown in green and yellow. The electrical path is indicated in dashed black line. HWP1, HWP2, half-wave plates; FI, Fabry isolator; SL, scan lens; M, mirror; TL, tube lens; DM1, DM2, dichroic mirrors; OBJ, objective; F1, F2, bandpass filters; PMT1, PMT2, photomultiplier tubes.

The laser beam is scanned by a pair of galvanometer-driven dual-axis scanning mirrors (GVS002, Thorlabs) at the focal plane (i.e., scan plane) of a scan lens (SL, AC254-045-B, Thorlabs, f_{SL} = 45 mm). After being focused by the scan lens, the laser beam is sent into a modified inverted microscope (IX71, Olympus), with some of its optical elements replaced to match the wavelength of the excitation source. In the microscope, the laser beam is collected and collimated by a tube lens (TL, Olympus, f_{TL} = 180 mm), which constitutes a 4*f* optical system with the scan lens. After passing a long-pass dichroic mirror (DM1, FF705-Di01, Semrock), the collimated beam is collected and focused into samples by a 20× 1.00NA water immersion objective (XLUMPLFLN, Olympus). Samples are placed on a three-dimensional motorized stage. The 4*f* optical system ensures that the beam will fill the back-aperture of the objective, and the middle plane of scanning mirrors and the pupil of the objective are mutually conjugate.

Signals from samples are collected by the objective in the epi-direction, separated from the laser beam by DM1, and detected by two channels (CH1, CH2) equipped with photomultiplier tubes (PMT1, PMT2). A combination of a long-pass dichroic mirror (DM2, FF470-Di01, Semrock) and two bandpass filters (F1, F2, FF02-435/40, FF01-565/133, Semrock) is applied to separate signals at different emission regions and minimize crosstalk between different channels. The achieved wavelength ranges are 415–455 nm and 495–635 nm for CH1 and CH2, respectively. A Labview based home-made microscope software simultaneously controls the scanner and restores images acquired from different detection channels.

3. RESULTS AND DISCUSSION

The capability of the simultaneous label-free TPF and SHG microscopy is demonstrated by using freshly excised mouse lung lobes. The schematic of mouse lower respiratory tract is shown in Figure 2(a). Figures 2(b) and 2(c) displays TPF and SHG images of mouse pulmonary alveoli.

As shown in Figure 2(a), the lower respiratory tract, along the proximal-distal axis, includes extrapulmonary airways (i.e., trachea and primary bronchi), intrapulmonary airways (i.e., lobar bronchi, segmental bronchi, subsegmental bronchi, and bronchioles) and alveolar regions. Alveolar regions are composed of alveoli and a network of capillaries. Alveoli are small air sacs inside lungs allowing air exchange. Along the luminal surface, an alveolus is lined by a cell layer of squamous type I pneumocytes and cuboidal type II pneumocytes. Type I pneumocytes provide an extensive surface area for air exchange, and type II pneumocytes secrete pulmonary surfactant proteins. The pneumocytes are anchored to the subjacent epithelial basement membrane, which is apposed and often fused to the endothelial basement membrane of a surrounding capillary. Endothelial cells of the capillary adhere closely to the endothelial basement membrane. There is interstitium between the two basement membranes, where a few stromal cells (e.g., fibroblasts) may be present[26]. The epithelial basement membrane, interstitium, and endothelial basement membrane compose the extracellular matrix of an alveolus. Two main components of the extracellular matrix are collagen and elastin fibers, which are responsible for the tensile strength and elastic modulus of alveoli, respectively. Collagen and elastin fibers can be revealed by contrast from SHG and autofluorescence, respectively. Fibroblasts in the interstitium keep synthesizing ground substance, as well as secreting collagen and elastin fibers, to maintain the integrity of extracellular matrix. Besides the main structures, a few macrophages also reside in the alveoli, which can be imaged by autofluorescence predominantly from lipids and flavins[27]. With similar structures, mouse alveoli are good models to investigate human alveoli[26,27].

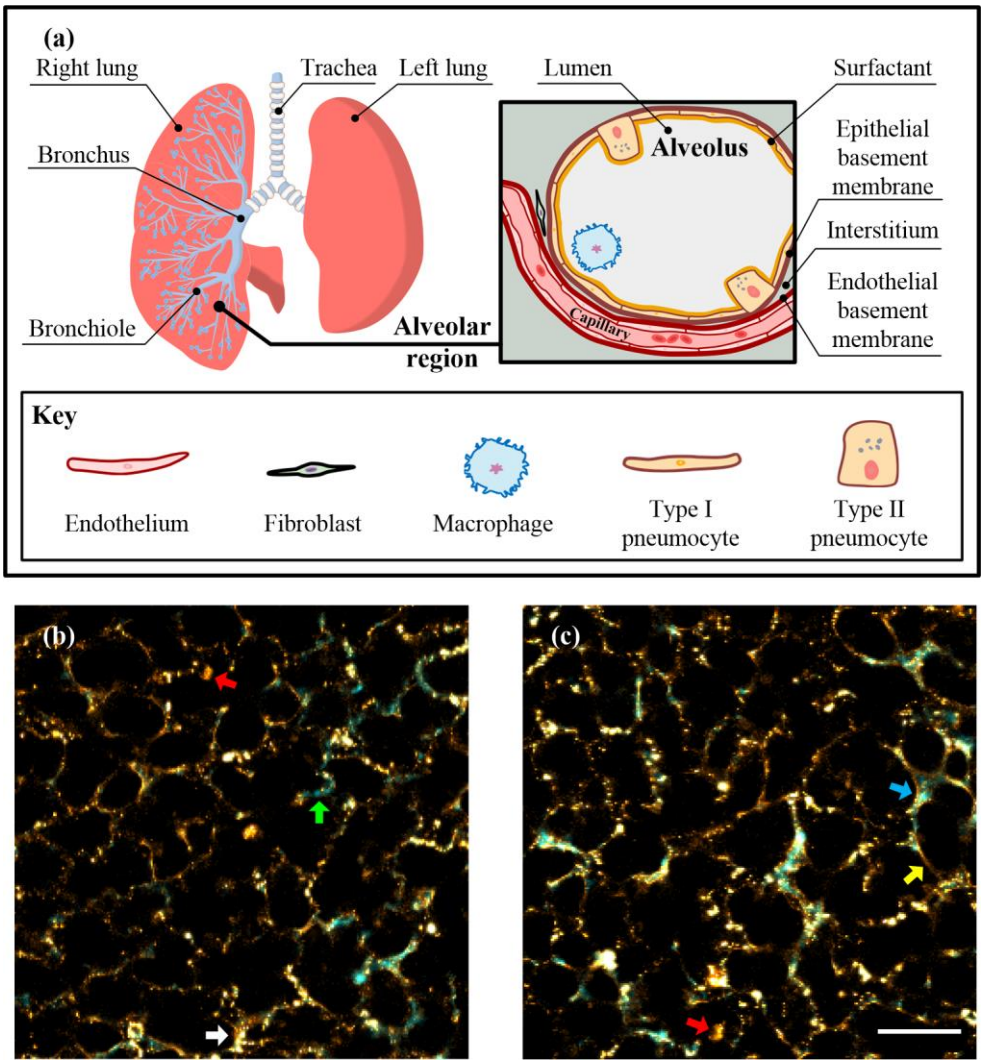

Figure 2. Demonstration of simultaneous label-free TPF and SHG microscopy of mouse pulmonary alveoli. (**a**) Schematic of mouse lower respiratory tract. The lower respiratory tract, along the proximal-distal axis, includes extrapulmonary airways, intrapulmonary airways, and alveolar regions. The alveolar regions are composed of several distinct layers, i.e., pneumocytes, epithelial basement membrane, interstitium, endothelial basement membrane, and endothelial cells. The pneumocytes are composed of type I pneumocytes responsible for air exchange and type II pneumocytes secreting surfactant proteins. A few macrophages may be present in the alveolar lumens or interstitium. Fibroblast can be found in the interstitium. (**b–c**) Simultaneously acquired TPF and SHG images of mouse pulmonary alveoli, 2 μs/pixel, 256×256 pixels. Cyan pixels (obtained from CH1) are mainly derived from prominent SHG of collagen. The green arrow in (b) indicates a pronounced bundle of collagen fibers. Yellow pixels (obtained from CH2) are mainly derived from autofluorescence of elastin, macrophages, and surfactant proteins. The yellow arrow in (c) denotes notable elastin fibers. The blue arrow in (c) shows that collagen fibers are attached to elastin fibers. The white arrow in (b) denotes surfactant proteins gathered probably in the cytoplasm of a type II pneumocyte. The red arrows in (b) and (c) indicate macrophages. The scale bar is 40 μm.

Simultaneously captured label-free TPF and SHG images of mouse alveoli are shown in Figures 2(b) and 2(c). The wavelength of the mode-locked Ti:Sapphire laser is tuned to 870 nm. At the focal plane, the excitation beam has an average power of approximately 15 mW. The images are acquired at the depth of approximately 30 μm into the pulmonary parenchyma. The detection channel CH1 is turned on to collect SHG around 435 nm, and CH2 is applied to detect TPF in the range of 495–635 nm. Cyan and yellow pixels in the images are obtained from CH1 and CH2, respectively. As shown in Figures 2(b) and 2(c), lumens of alveoli filled with air are apparent. Cyan pixels may be predominantly contributed by prominent SHG from collagen fibers in the alveolar extracellular matrix. Yellow pixels may be mainly derived from autofluorescence of elastin, macrophages, and surfactant proteins. In Figure 2(b), the green

arrow in indicates a notable bundle of collagen fibers. The white arrow denotes a location of gathered cyan granules, which are most likely derived from autofluorescence of surfactant proteins on the luminal surfaces (probably inside the cytoplasm of type II pneumocytes). In Figure 2(c), yellow pixels denoted by the yellow arrow are attributed to be elastin fibers, according to their typical rope-like structures. The round-shaped yellow object indicated by the red arrow may correspond to a macrophage. The endogenous contrasts of elastin fibers and macrophages are predominantly contributed by autofluorescence emission at 495 nm to 635 nm, which is similar with previously published data[28]. The blue arrow depicts that collagen bundles are attached to elastin fibers. This structural feature confirms that elastin fibers and collagen bundles are actually separate structures, though their signals seem to overlap in some pixels. Scattered yellow granules around collagen and elastin fibers can be found in both Figures 2(b) and 2(c), which are probably contributed by autofluorescence derived from lipopigments and flavins in fibroblasts. The experimental results confirm that simultaneous TPF and SHG microscopy is capable of revealing the microenvironment of mouse pulmonary alveoli.

4. CONCLUSIONS

The simultaneous label-free TPF and SHG imaging system has the advantages of acquiring more information from unstained biological samples than using only one nonlinear imaging modality, and avoiding possible artifacts from sample motion or laser power fluctuation. Simultaneous autofluorescence and SHG images of unstained mouse pulmonary alveoli are acquired with the pixel dwell time of 2 μs. At 870 nm excitation, images of pulmonary alveoli distinctly reveal the microenvironment by autofluorescence from elastin fibers and SHG from collagen fibers. Two other components of alveoli are also visualized by TPF, which are macrophages residing inside apparent alveolar lumens and surfactant proteins gathered probably inside the cytoplasm of type II pneumocytes. These demonstrated experimental results indicate that the simultaneous TPF and SHG imaging system is suitable for visualizing the morphologies of biological tissues, and it has the potential to monitor physiological processes and investigate structure-related diseases.

REFERENCES

[1] Helmchen, F. and Denk, W., "Deep tissue two-photon microscopy," Nat. Methods 2(12), 932–940 (2005).
[2] So, P. T., Dong, C. Y., Masters, B. R. and Berland, K.M., "Two-photon excitation fluorescence microscopy," Annu. Rev. Biomed. Eng. 2, 399–429 (2000).
[3] Xia, F., Wu, C., Sinefeld, D., Li, B., Qin, Y. and Xu, C, "*In vivo* label-free confocal imaging of the deep mouse brain with long-wavelength illumination," Biomed Opt. Express 9(12), 6545–6555 (2018).
[4] Wilson, T., "Resolution and optical sectioning in the confocal microscope," J. Microsc. 244(2), 113–121 (2011).
[5] Karpf, S., Eibl, M., Sauer, B., Reinholz, F., Huttmann, G. and Huber, R., "Two-photon microscopy using fiber-based nanosecond excitation," Biomed Opt. Express 7(7), 2432–2440 (2016).
[6] Podgorski, K. and Ranganathan, G., "Brain heating induced by near-infrared lasers during multiphoton microscopy," J. Neurophysiol. 116(3), 1012–1023 (2016).
[7] Xia, F., Wu, C., Sinefeld, D., Li, B., Qin, Y. and Xu, C, "*In vivo* label-free confocal imaging of adult mouse brain up to 1.3-mm depth with NIR-II illumination," Proc. SPIE 10865, 1086504 (2019).
[8] Zipfel, W. R., Williams, R. M. and Webb, W. W., "Nonlinear magic: multiphoton microscopy in the biosciences," Nat. Biotechnol. 21(11), 1369–1377 (2003).
[9] Mertz, J., "Nonlinear microscopy: new techniques and applications," Curr. Opin. Neurobiol. 14(5), 610–616 (2004).
[10] Denk, W., Strickler, J. H. and Webb, W. W., "Two-photon laser scanning fluorescence microscopy," Science 248(4951), 73–76 (1990).
[11] Niederriter, R. D., Ozbay, B. N., Futia, G. L., Gibson, E. A. and Gopinath, J. T., "Compact diode laser source for multiphoton biological imaging," Biomed. Opt. Express 8(1), 315–322 (2017).
[12] Isobe, K., Watanabe, W., Matsunaga, S., Higashi, T., Fukui, K. and Itoh, K., "Multi-spectral two-photon excited fluorescence microscopy using supercontinuum light source," Jpn. J. Appl. Phys. 44(4), L167–L169 (2005).
[13] Unruh, J. R., Price, E. S., Gagliano, M. R., Stehno-Bittek L., Johnson, C. K. and Hui, R., "Two-photon microscopy with wavelength switchable fiber laser excitation," Opt. Express 14(21), 9825–9831 (2006).
[14] Ouzounov, D. G., Wang, T., Wang, M., Feng, D. D., Horton, N. G., Cruz-Hernández, J. C., Cheng, Y.-T., Reimer, J., Tolias, A. S., Nishimura, N. and Xu, C., "*In vivo* three-photon imaging of activity of GCaMP6-labeled neurons deep in intact mouse brain," Nat. Methods 14(4), 388–390 (2017).

[15] Li, B., Wu, C., Wang, M., Charan, K. and Xu, C., "An adaptive excitation source for high-speed multiphoton microscopy," Nat. Methods 17, 163–166 (2020).
[16] Mohler, W., Millard, A. C. and Campagnola, P. J., "Second harmonic generation imaging of endogenous structural proteins," Methods 29(1), 97–109 (2003).
[17] Burke, K. A., Dawes, R. P., Cheema, M. K., Van Hove, A., Benoit, D. S. W., Perry, S. W. and Brown, E., "Second harmonic generation scattering directionality predicts tumor cell motility in collagen gels," J. Biomed. Opt. 20(5), 051024 (2015).
[18] Harpel, K., Baker, R. D., Amirsolaimani, B. A., Mehravar, S., Vagner, J., Matsunaga, T. O., Banerjee, B. and Kieu, K., "Imaging of targeted lipid microbubbles to detect cancer cells using third harmonic generation microscopy," Biomed. Opt. Express 7(7), 2849–2860 (2016).
[19] Qin, Y., Li, B., Xia, F., Xia, Y. and Xu, C., "Time-lens based multi-color background-free coherent anti-Stokes Raman scattering microscopy," Proc. SPIE 10890, 108901U (2019).
[20] Qin, Y., Li, B., Xia, F., Xia, Y. and Xu, C., "Multi-color background-free coherent anti-Stokes Raman scattering microscopy using a time-lens source," Opt. Express 26(26), 34474–34483 (2018).
[21] Li, J., Lin, P., Tan, Y. and Cheng, J.-X., "Volumetric stimulated Raman scattering imaging of cleared tissues towards three-dimensional chemical histopathology," Biomed. Opt. Express 10(8), 4329–4339 (2019).
[22] Stringari, C., Edwards, R. A., Pate, K. T., Waterman, M. L., Donovan, P. J. and Gratton, E., "Metabolic trajectory of cellular differentiation in small intestine by phasor fluorescence lifetime microscopy of NADH," Sci. Rep. 2, 568 (2012).
[23] Pena, A. M., Fabre, A., Débarre, D., Marchal-Somme, J., Crestani, B., Martin, J. L., Beaurepaire, E. and Schanne-Klein, M. C., "Three-dimensional investigation and scoring of extracellular matrix remodeling during lung fibrosis using multiphoton microscopy," Microsc. Res. Technq. 70(2), 162–170 (2007).
[24] Qin, Y., Li, Q., Xia, Y., Liu, B. and Zhang, S., "Construction and application of femtosecond laser two-photon fluorescence microscopy system," Journal of Harbin Institute of Technology 47(11), 1–5 (2015).
[25] Wang, S., Qin, Y., Guo, M., Zhang, S. and Xia, Y., "High speed 3D two-photon fluorescence microscopy by femtosecond laser pulses," Proc. SPIE 10605, 106053J (2017).
[26] Barkauskas, C. E., Chung, M.-I., Fioret, B., Gao, X., Katsura, H. and Hogan, B. L. M., "Lung organoids: current uses and future promise," Development 144(6), 986–997 (2017).
[27] Rock, J. R., Randell, S. H. and Hogan, B. L. M., "Airway basal stem cells: a perspective on their roles in epithelial homeostasis and remodeling," Dis. Model. Mech. 3, 545–556 (2010).
[28] Zipfel, W. R., Williams, R. M., Christie, R., Nikitin, A. Y., Hyman, B. T. and Webb, W. W., "Live tissue intrinsic emission microscopy using multiphoton-excited native fluorescence and second harmonic generation," Proc. Natl. Acad. Sci. 100(12), 7075–7080 (2003).